

A simple, entropy-based dissipation trigger for SPH

S. Rosswog^{*1}

¹ *The Oskar Klein Centre, Department of Astronomy, Stockholm University, AlbaNova, SE-106 91 Stockholm, Sweden*

Draft version

ABSTRACT

Smoothed Particle Hydrodynamics (SPH) schemes need to be enhanced by dissipation mechanisms to handle shocks. Most SPH formulations rely on artificial viscosity and while this working well in pure shocks, attention has to be paid to avoid dissipation where it is not wanted. Commonly used approaches include limiters and time-dependent dissipation parameters. The former try to distinguish shocks from other types of flows that do not require dissipation while in the latter approach the dissipation parameters are steered by some source term (“trigger”) and, if not triggered, they decay to a pre-described floor value. The commonly used source terms trigger on either compression, $-\nabla \cdot \vec{v}$, or its time derive. Here we explore a novel way to trigger SPH-dissipation: since an ideal fluid conserves entropy exactly, its numerical non-conservation can be used to identify “troubled particles” that need dissipation because they either pass through a shock or become noisy for other reasons. Our new scheme is implemented into the Lagrangian hydrodynamics code `MAGMA2` and is scrutinized in a number of shock and fluid instability tests. We find excellent results in shocks and only a very moderate (and desired) switch-on in instability tests. The new scheme is robust, trivial to implement into existing SPH codes and does not add any computational overhead.

1 INTRODUCTION

Smoothed Particle Hydrodynamics (Lucy 1977; Monaghan 1977) is a completely mesh-free method to solve the equations of hydrodynamics. It can be elegantly derived from a discretized Lagrangian of an ideal fluid (Gingold & Monaghan 1982; Speith 1998; Monaghan & Price 2001; Springel & Hernquist 2002; Rosswog 2015b) and thus ensures that Nature’s conservation laws are obeyed. As derived in this way, SPH is entirely dissipationless, and can therefore not handle shocks: in a shock front bulk kinetic energy is transformed by dissipation into internal energy which goes along with an increase in entropy. Therefore, the ideal SPH equations need to be enhanced by some dissipative mechanism. In most modern Eulerian hydrodynamics schemes this is achieved by applying (exact or approximate) Riemann solvers, see e.g. Toro (1999). This is also possible in SPH (Inutsuka 2002; Cha & Whitworth 2003; Puri & Ramachandran 2014), but the use of artificial viscosity is more widespread. It is worth mentioning, however, that many artificial viscosity schemes bear similarities with approximate Riemann solvers (Monaghan 1997). While Riemann solvers are an elegant concept and less ad hoc than artificial viscosity, they always provide some amount of dissipation even in situations where it would actually not be needed. In SPH one has (at least in principle) the possibility to suppress/switch off dissipation completely. Historically, however, early implementations applied artificial viscosity terms with constant parameters and without limiters so that dissipation was always switched on whether needed or not. This led to excessively dissipative SPH schemes and controlling the amount of dissipation has been a concern since.

Suggested cures include “limiters” (Balsara 1995; Cullen & Dehnen 2010; Read & Hayfield 2012; Wadsley et al. 2017) that are aimed at suppressing dissipation outside of shocks, tensor prescriptions (Owen 2004) that intend to restrict the effects of artificial vis-

cosity to the shock travel directions and dissipation schemes with time dependent parameters. Time dependent dissipation parameters were introduced by Morris & Monaghan (1997) who suggested to evolve them separately for each particle according to an additional differential equation with a source and a decay term that, unless triggered, drive the parameter to a pre-defined small floor value, see Eq. (17) below. As a source term they used $-\nabla \cdot \vec{v}$ which works well in many cases, but cannot distinguish between an adiabatic compression and an entropy producing shock. Cullen & Dehnen (2010) suggested to use instead $d(-\nabla \cdot \vec{v})/dt$ as a dissipation trigger, so that a particle that moves into a shock (and thereby becomes increasingly more compressed) raises its dissipation parameter which subsequently decays once the shock wave has passed.

Here we explore an alternative trigger that involves keeping track of some entropy measure at the particle level. Monitoring entropy violations has been used to steer dissipation in Eulerian Newtonian hydrodynamics (Guermond et al. 2011, 2016) and it has also been used in relativistic hydrodynamics to steer to which amount low-order fluxes need to be added to higher-order fluxes for numerical stabilization (Guercilena et al. 2017). In this paper we use the local violation of exact entropy conservation to steer how much dissipation every SPH-particle needs. As shown in the tests below, our scheme yields excellent results, is trivial to implement and comes without any computational overhead. We describe our methodology in Sec. 2, where we also briefly summarize the key ingredients of our `MAGMA2` code in Sec. 2.1, and we discuss the entropy dissipation trigger in Sec. 2.2. In Sec. 3 we show a number of benchmark tests and we conclude in Sec. 4 with a concise summary.

arXiv:1912.01095v2 [astro-ph.IM] 10 Jun 2020

2 METHODOLOGY

2.1 The Smoothed Particle Hydrodynamics formulation

The SPH code `MAGMA2` (Rosswog 2020) profits from a number of new elements: a) it uses of high order kernels, b) calculates accurate gradients via matrix inversion techniques and c) uses a new dissipation scheme where velocities are reconstructed via slope limiter techniques to the inter-particle midpoint (Christensen 1990; Frontiere et al. 2017). The differences of these reconstructed velocities are used in the artificial viscosity tensor rather than the (“flat”) differences of the particle velocities, as is the standard practice in SPH. This approach drastically reduces unwanted dissipation and we have shown in an extensive set of test cases (Rosswog 2020) that excellent results are obtained even if the dissipation parameter α is kept constant at its maximum value. This finding is consistent with the results of Frontiere et al. (2017) who used an SPH formulation based on reproducing kernel interpolation (Liu et al. 1995). The main aim of this study is to apply dissipation only to “troubled particles” that are identified via entropy non-conservation between two subsequent time steps.

The equation set that we are using has been developed and tested extensively in a special relativistic context (Rosswog 2015a) and – in its Newtonian version – in the recent `MAGMA2` code paper (Rosswog 2020). We use

$$\rho_a = \sum_b m_b W_{ab}(h_a), \quad (1)$$

$$\frac{d\vec{v}_a}{dt} = -\sum_b m_b \left\{ \frac{P_a}{\rho_a^2} \vec{G}_a + \frac{P_b}{\rho_b^2} \vec{G}_b \right\}, \quad (2)$$

$$\left(\frac{du_a}{dt} \right) = \frac{P_a}{\rho_a^2} \sum_b m_b \vec{v}_{ab} \cdot \vec{G}_a, \quad (3)$$

as density, momentum and energy equation, where ρ , \vec{v}_a , u_a denote mass density, velocity and specific internal energy, m is the particle mass, P the gas pressure, $\vec{v}_{ab} = \vec{v}_a - \vec{v}_b$, W the chosen SPH kernel function and h its smoothing length. The gradient functions are given by

$$\left(\vec{G}_a \right)^k = \sum_{d=1}^D C^{kd}(\vec{r}_a, h_a) (\vec{r}_b - \vec{r}_a)^d W_{ab}(h_a), \quad (4)$$

$$\left(\vec{G}_b \right)^k = \sum_{d=1}^D C^{kd}(\vec{r}_b, h_b) (\vec{r}_b - \vec{r}_a)^d W_{ab}(h_b), \quad (5)$$

where C is a “correction matrix” that accounts for the local particle distribution and is calculated as

$$\left(C_a^{kd}(h) \right) = \left(\sum_b \frac{m_b}{\rho_b} (\vec{r}_b - \vec{r}_a)^k (\vec{r}_b - \vec{r}_a)^d W(|\vec{r}_a - \vec{r}_b|, h) \right)^{-1}. \quad (6)$$

Such gradients have been shown to work well (Garcia-Senz et al. 2012; Cabezon et al. 2012) and to be orders of magnitude more accurate than standard SPH-kernel gradient methods, see Fig. 1 in Rosswog (2015a). Following the approach of von Neumann & Richtmyer (1950), we implement artificial viscosity by adding an “artificial pressure” Q to the physical pressure P wherever it occurs. We use the expression (Monaghan & Gingold 1983)

$$Q_a = \alpha \rho_a \left(-c_{s,a} \mu_a + 2\mu_a^2 \right), \quad (7)$$

where the velocity jump is (summation over δ)

$$\mu_a = \min \left(0, \frac{v_{ab}^\delta \eta_a^\delta}{\eta_a^2 + \varepsilon^2} \right). \quad (8)$$

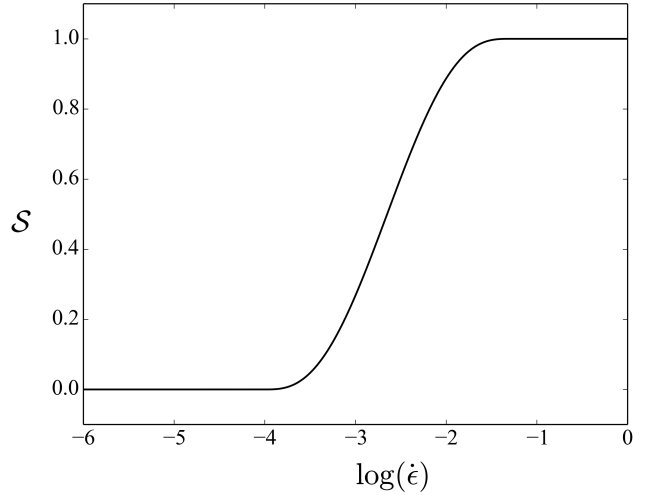


Figure 1. The smooth switch-on function that we use to translate entropy violations into dissipation parameter values, see Eq. (19).

The numerical parameters α and ε are usually set to 1 and 0.1, $c_{s,a}$ is the sound speed and

$$\eta_a^\delta = \frac{(\vec{r}_a - \vec{r}_b)^\delta}{h_a}, \quad \eta_a^2 = \eta_a^\delta \eta_a^\delta \quad (9)$$

are (non-dimensionalized) separations between particles. In SPH it is common practice to use $v_{ab}^\delta = \vec{v}_a^\delta - \vec{v}_b^\delta$ in Eq. (8), i.e. to apply the velocity difference between the two particles. In `MAGMA2` we quadratically reconstruct the velocities of particle a and b to their midpoint at $\vec{r}_{ab} = 0.5(\vec{r}_a + \vec{r}_b)$, so that the velocities reconstructed from the a -side read

$$\vec{v}_a^i = v_a^i + \Phi_{ab} \left[(\partial_j v^i) \delta^j + \frac{1}{2} (\partial_l \partial_m v^i) \delta^l \delta^m \right]_a, \quad (10)$$

where the index at the square bracket indicates that the derivatives at the position of particle a are used and the increments from point a to the midpoint are $(\delta^j)_a = \frac{1}{2}(\vec{r}_b - \vec{r}_a)$. The reconstructed velocities from the b -side, \vec{v}_b^i , are calculated correspondingly, but with derivatives from position b and increments $\delta_b^i = -\delta_a^i$. In Eq. (8) we use the difference in the *reconstructed* velocities, i.e. $v_{ab}^\delta = \vec{v}_a^\delta - \vec{v}_b^\delta$. To calculate the first and second velocity derivatives we also use matrix inversion techniques, see Rosswog (2020) for more details.

We use a modification of van Leer’s slope limiter (van Leer 1974; Frontiere et al. 2017)

$$\Phi_{ab} = \max \left[0, \min \left[1, \frac{4A_{ab}}{(1+A_{ab})^2} \right] \right] \begin{cases} 1, & \text{if } \eta_{ab} > \eta_{\text{crit}} \\ e^{-\left(\frac{\eta_{ab} - \eta_{\text{crit}}}{0.2} \right)^2}, & \text{otherwise} \end{cases} \quad (11)$$

with

$$A_{ab} = \frac{(\partial_\delta v_a^\gamma) x_{ab}^\delta x_{ab}^\gamma}{(\partial_\delta v_b^\gamma) x_{ab}^\delta x_{ab}^\gamma} \quad (12)$$

and

$$\eta_{ab} = \min(\eta_a, \eta_b) = \min \left(\frac{r_{ab}}{h_a}, \frac{r_{ab}}{h_b} \right) \text{ and } \eta_{\text{crit}} = \left(\frac{32\pi}{3N_{\text{nei}}} \right)^{1/3}, \quad (13)$$

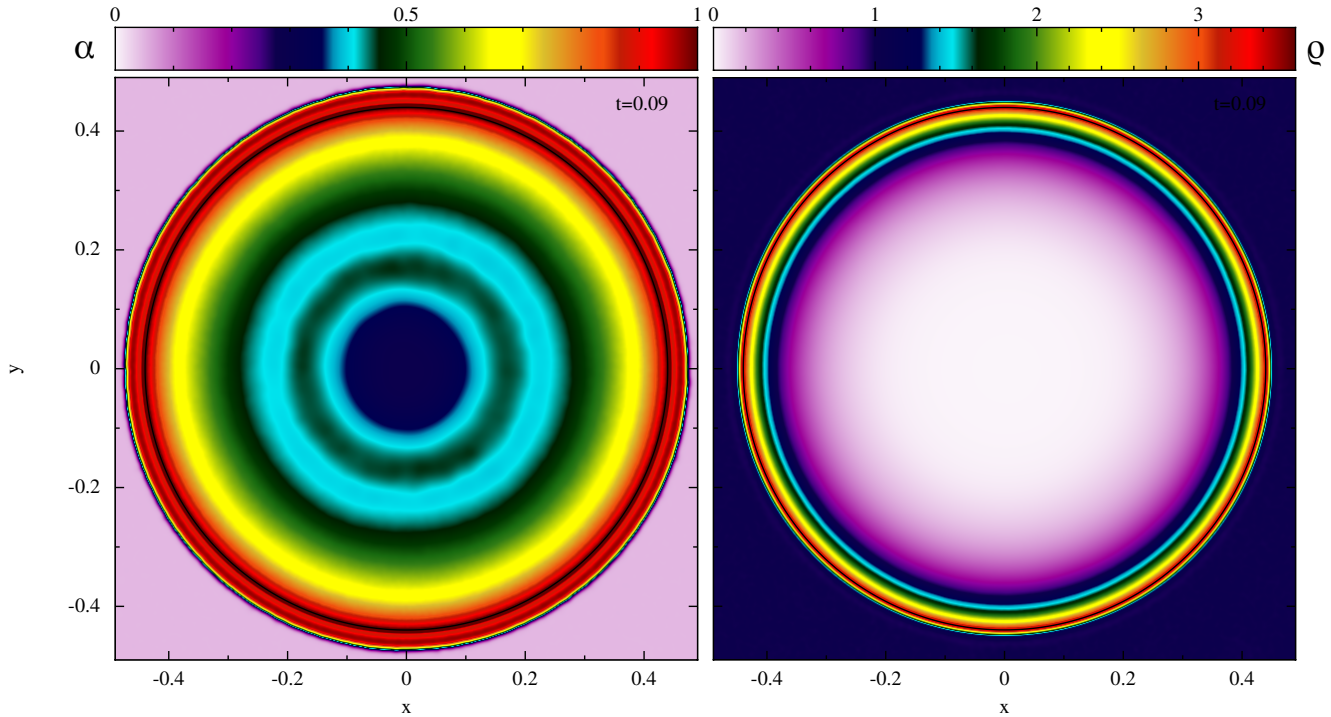


Figure 2. 3D Sedov test (200^3 particles), dissipation parameter α on the left and density ρ on the right at $t = 0.09$.

with N_{nei} being the number of neighbours for the chosen kernel. We also apply a small amount of thermal conductivity

$$\left(\frac{du_a}{dt}\right)_C = -\alpha_u \sum_b m_b \frac{v_{\text{sig},u}^{ab}}{\rho_{ab}} (u_a - u_b) \frac{|\vec{G}_a + \vec{G}_b|}{2}, \quad (14)$$

where $\alpha_u = 0.05$ and $v_{\text{sig},u}$ is a signal velocity. For more details and the explicit expressions that we use we refer to the `MAGMA2` code paper (Rosswog 2020). In all of the shown tests we use the Wendland C6 kernel (Wendland 1995) with 300 neighbour particles.

2.2 Using entropy non-conservation to identify “troubled particles”

Our SPH formulation conserves mass energy, momentum and angular momentum exactly¹, entropy conservation, in contrast, is not actively enforced and therefore its potential non-conservation can be used to monitor the smoothness of the local flow. In smooth flows entropy should be conserved exactly while it may be physically increased in shocks. Flows can, however, also become “noisy” (i.e. non-negligible velocity fluctuations appear) for numerical reasons (e.g. particles moving off an initially specified, non-optimal lattice) and also in such cases (a smaller amount of) dissipation is desirable. In either case, shocks or noisy flows, one would want to apply artificial dissipation in order to keep the flow physically well-behaved, and measuring the degree of numerical non-conservation of entropy (or some entropy function) is a natural way to identify “troubled particles” and to determine how much dissipation should

be applied.

Here we suggest to measure the *rate* of numerical entropy generation between two subsequent time steps and a translation of this rate into a value for the dissipation parameter α . Since `MAGMA2` produces, due to the velocity reconstruction, excellent results even with a constant $\alpha = 1$, we choose our parameters conservatively large so that α reaches already substantial values for small entropy violations. For SPH schemes without such a velocity reconstructions the same functional relations can be used, but the optimal parameter values may have slightly different values.

We assume here a polytropic equation of state and use

$$s_a \equiv \frac{P_a}{\rho_a^\Gamma} \quad (15)$$

as a measure for the entropy carried by particle a . Here P_a is the gas pressure and Γ the polytropic exponent. Polytropic equations of state are used in most astrophysical gas simulations, but other entropy measures, e.g. the physical entropy of an ideal gas, could equally well be used along the same lines of reasoning. Even if other sources of entropy (e.g. nuclear reactions) should be present, this approach can be used provided that one can cleanly separate out the contributions from the additional source. But this is not the topic of our study here and we leave this for future investigations.

We use the non-dimensionalized relative entropy rate of change of a particle a between time step t^{n-1} and time step t^n ($\Delta t = t^n - t^{n-1}$)

$$\epsilon_a^n \equiv \frac{|s_a^n - s_a^{n-1}|}{s_a^{n-1}} \frac{\tau_a}{\Delta t}, \quad (16)$$

as a measure of how much dissipation is needed. Here $\tau_a = h_a/c_{s,a}$ is the particle’s dynamical time scale and $c_{s,a}$ its sound speed. We use $l_a^n \equiv \log(\epsilon_a^n)$ to steer the amount of dissipation. Similar to earlier work (Morris & Monaghan 1997; Rosswog et al. 2000; Cullen &

¹ Modulo effects from the grad-h effects, potential finite accuracy in the ODE integration and approximations for gravitational forces etc.

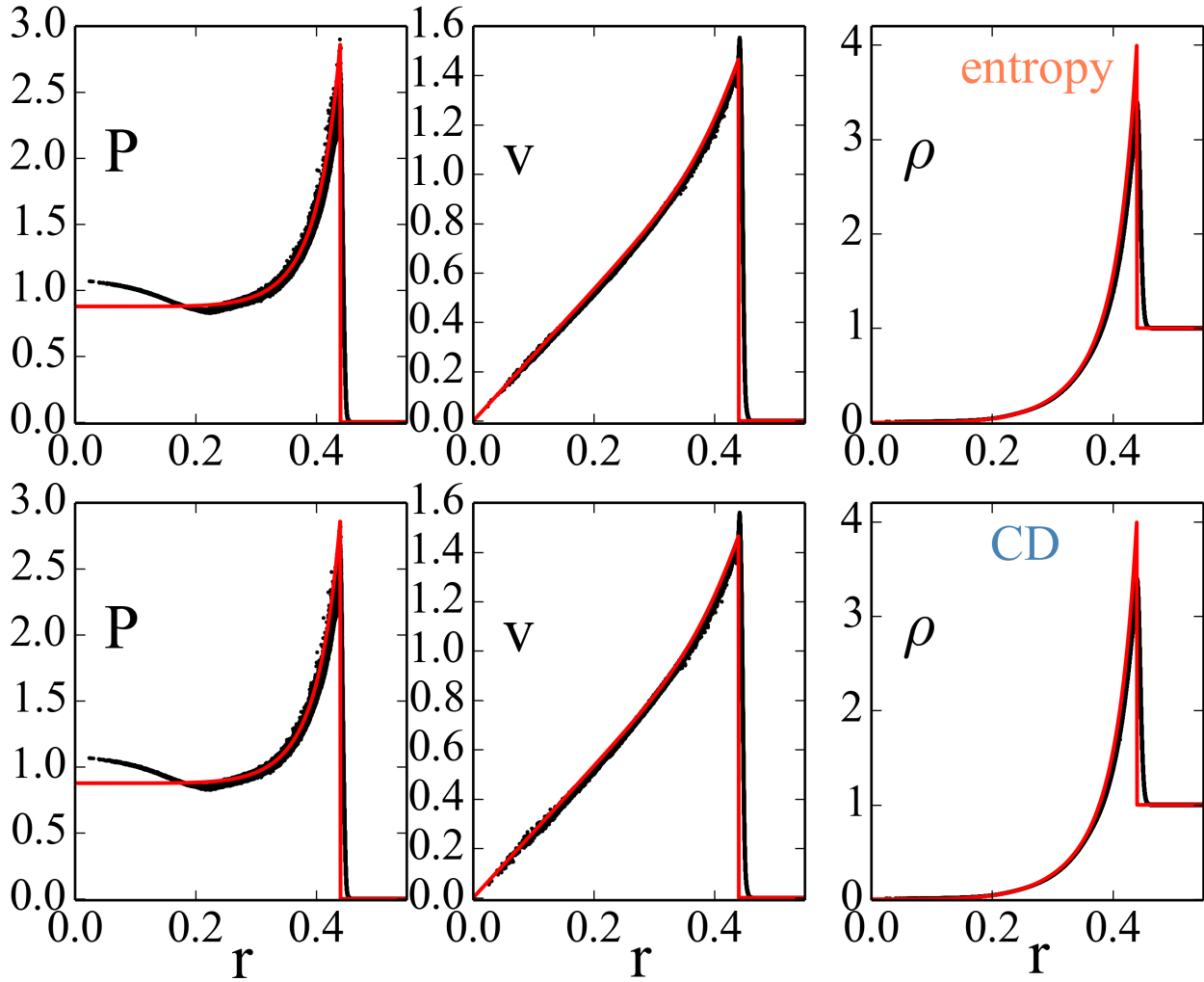


Figure 3. 3D Sedov test (200^3 particles, at $t = 0.09$); upper row: the suggested entropy-steering; lower row: $d(\nabla \cdot \vec{v})/dt$ -steering. Each time pressure P (left), velocity v (middle) and density ρ (right), all particles (black) and the exact solution (red) are shown.

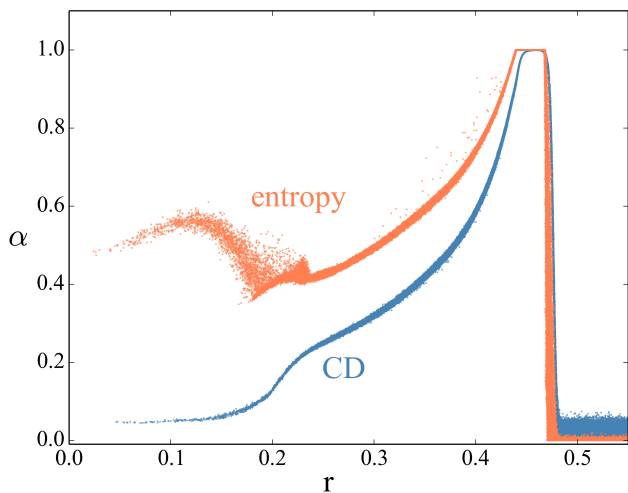


Figure 4. Comparison of the triggered dissipation parameter values in 3D Sedov test (200^3 particles) between the proposed scheme (“entropy”) and the $d(\nabla \cdot \vec{v})/dt$ trigger (CD).

Dehnen 2010; Rosswog 2015a; Wadsley et al. 2017), we let the dissipation parameter α_a decay according to

$$\frac{d\alpha_a}{dt} = -\frac{\alpha(t) - \alpha_0}{30\tau_a}, \quad (17)$$

where α_0 is a floor value, in other schemes often set to values around 0.1 to keep the particle distribution well-behaved (Tricco 2019). Note that we have conservatively chosen a rather long decay time scale of $30\tau_a$. We compare at each time step the actual value to a “desirable dissipation parameter” and if the latter exceeds the current value, $\alpha(t)$ is increased instantly (Cullen & Dehnen 2010). The desired value of α is chosen according to the trigger l_a^n

$$\alpha_{a,\text{des}}^n = \alpha_{\text{max}} S(l_a^n), \quad (18)$$

where S is smooth “switch-on” function for which we have chosen, see Fig. 1,

$$S(x) = 6x^5 - 15x^4 + 10x^3, \quad (19)$$

with

$$x = \min \left[\max \left(\frac{l_a^n - l_0}{l_1 - l_0}, 0 \right), 1 \right]. \quad (20)$$

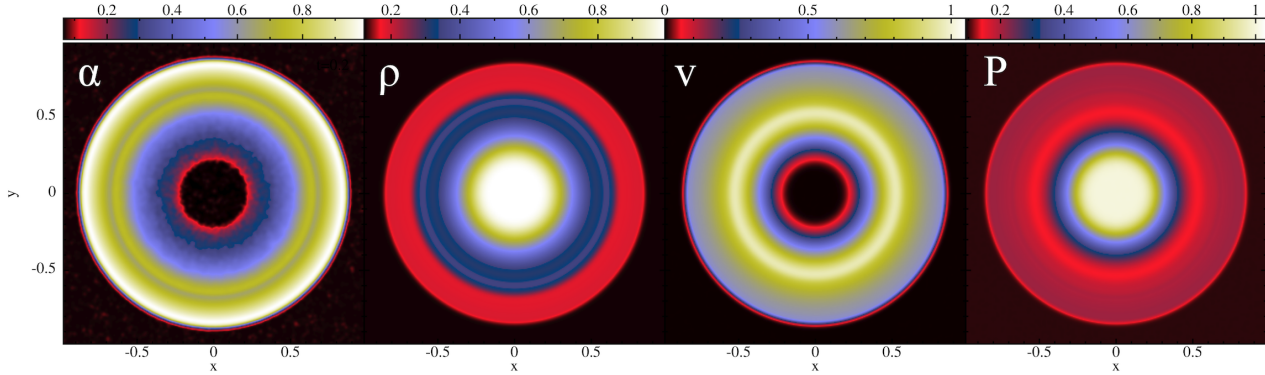


Figure 5. Spherical Riemann problem in 3D with entropy trigger. From left to right: dissipation parameter α , density ρ , velocity v and pressure P .

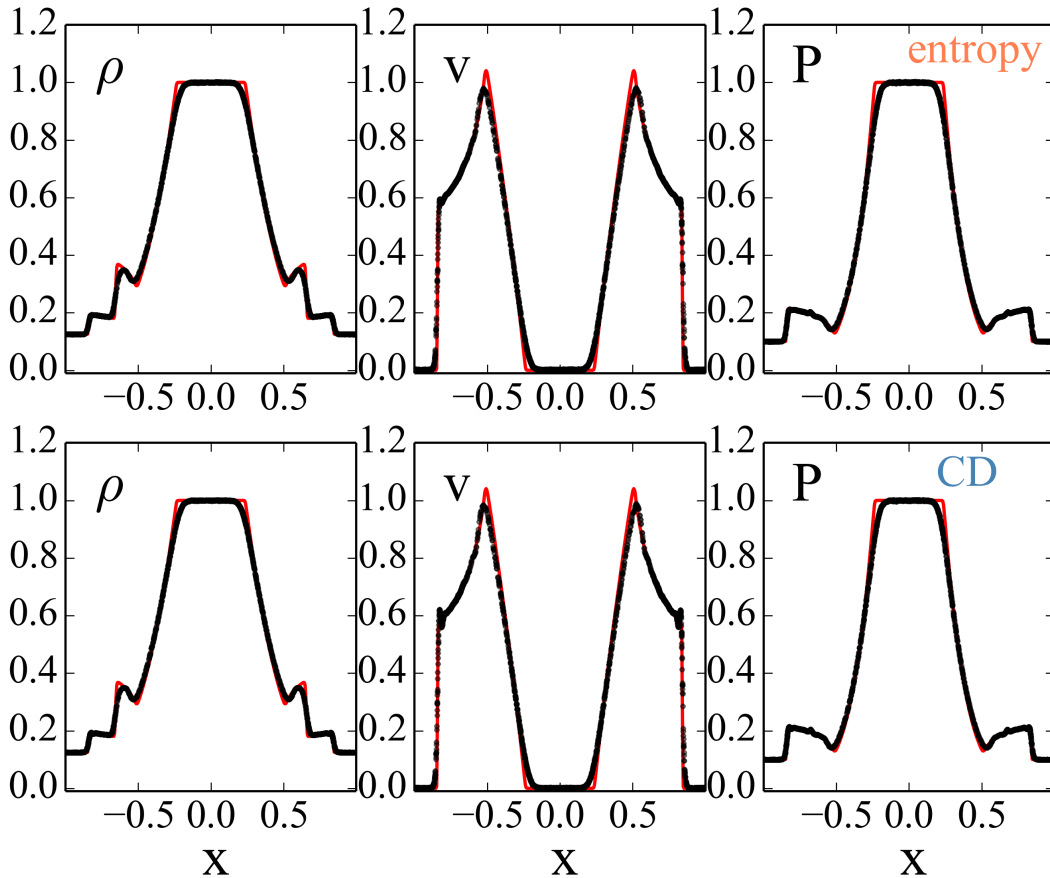


Figure 6. Spherical Riemann problem in 3D: the MAGMA2 solution (200^3 particles) is shown as black circles, the reference solution (red line) has been obtained with the Eulerian weighted average flux method with 400^3 grid cells (Toro 1999). The upper row shows the results from the entropy trigger, the lower one is obtained using the $d(\nabla \cdot \vec{v})/dt$ -trigger.

The reasoning behind this is that we consider dissipation unnecessary for acceptably small entropy violations (exact value set by l_0) and beyond another threshold value (set by l_1) we need the maximal dissipation parameter, α_{\max} . After some experimenting with both shocks and instability tests, we settled on values $l_0 = \log(1 \times 10^{-4})$ and $l_1 = \log(5 \times 10^{-2})$, so that our scheme does not switch on at all for entropy violations $\dot{\epsilon}_a^n \leq 10^{-4}$ and reaches $\alpha = \alpha_{\max} = 1$ for

$\dot{\epsilon}_a^n \geq 5 \times 10^{-2}$, see Fig. 1. For aesthetic reasons we prefer to have only *triggered* dissipation rather than assigning a floor value α_0 by hand. We therefore use $\alpha_0 = 0$ in our implementation, but note that with the chosen parameters l_0 and l_1 a small amount of dissipation (typically $\alpha \sim 0.01$) is triggered even in smooth flows, see below. We find good results for this particular switch-on function and the chosen parameters, but other choices are certainly possible and the

6 Rosswog

optimal parameter values might be slightly different for other SPH formulations.

In the below tests, we compare also to the $d(\nabla \cdot \vec{v})/dt$ -trigger suggested by Cullen & Dehnen (2010). Here the desired dissipation parameter is chosen as²

$$\alpha_{a,\text{des}}^{n,\text{CD}} = \frac{A_a}{0.25 \left(\frac{v_{a,\text{sig}}}{h_a} \right)^2 + A_a}, \quad (21)$$

where $A = \min(-d(\nabla \cdot \vec{v})/dt, 0)$ and the signal velocity is given by

$$v_{a,\text{sig}} = \max_b [c_{s,ab} - \min\{0, \vec{v}_{ab} \cdot \hat{e}_{ab}\}]. \quad (22)$$

Here, $c_{s,ab} = 0.5(c_{s,a} + c_{s,b})$, $\vec{v}_{ab} = \vec{v}_a - \vec{v}_b$ and $\hat{e}_{ab} = (\vec{r}_a - \vec{r}_b)/|\vec{r}_a - \vec{r}_b|$. Cullen & Dehnen (2010) chose a decay time scale of $20h_a/v_{a,\text{sig}}$ for the denominator of Eq. (17) and this is the parameter we adopt in this comparison. It is worth pointing out that this is a comparison of *triggers* and there are differences between our approach with the $d(\nabla \cdot \vec{v})/dt$ -trigger (e.g. SPH-formulation, kernels, reconstruction, conductivity) and the original Cullen & Dehnen approach. Nevertheless, we use the "CD" in some of the below figures as a shorthand for this $d(\nabla \cdot \vec{v})/dt$ -trigger approach.

3 TESTS

To scrutinize the suggested scheme, we perform a number of benchmark tests. We perform shock tests to demonstrate that the dissipation robustly switches on and avoids spurious oscillations and Kelvin-Helmholtz and Rayleigh-Taylor tests to verify that no unnecessary dissipation is triggered in smooth portions of the flow.

3.1 Sedov Taylor Blast

We begin by setting up a Sedov explosion test where a given number of SPH particles is distributed according to a centroidal Voronoi tessellation (Du et al. 1999) in the computational volume $[-0.5, 0.5] \times [-0.5, 0.5] \times [-0.5, 0.5]$. While this already produces very good quality initial conditions, they can be further improved by applying regularization sweeps, where each particle position is corrected according to Eq. (20) of Gaburov & Nitadori (2011). This procedure ensures nearly perfectly spherically symmetric results in this test. Subsequently we assign masses so that the density is $\rho = 1$. We use a polytropic exponent $\Gamma = 5/3$ and spread an internal energy $E = 1$ across a very small initial radius R , the specific internal energy u of the particles outside of R is entirely negligible (10^{-10} of the central u). For the initial radius R we choose twice the interaction radius of the innermost SPH particle. Boundaries play no role in this test (as long as the blast doesn't interact with them), we therefore place "frozen" particles with fixed properties around the computational volume as boundary particles. For more details we refer to Rosswog (2020).

We show in Fig. 2 the dissipation parameter α (left) and the density ρ (right) for 200^3 SPH particles (excluding boundary particles). This test requires large dissipation values, both to robustly handle the shock and to "calm" the particles in the post-shock region. Our scheme delivers large α -values in this test with values of ≈ 1 in the shock itself, and a moderate decay to values around 0.4 in the shocked, inner region. We show in Fig. 3, upper row, the numerical solution of pressure, velocity and density (black dots)

as a function of radius together with the exact solution (red). Note that *all* particles are plotted. Keep in mind that this numerical test challenges most methods whether particle- or mesh-based and often noise and strong spurious post-shock oscillations occur, see for example Rosswog & Price (2007); Hu et al. (2014); Cardall et al. (2014); Hopkins (2015); Wadsley et al. (2017) or Frontiere et al. (2017). For our results, the overall agreement is very good and there is only a small velocity overshoot at the shock and –since the finite particle masses– overestimate the close-to-zero central density, the central pressure is somewhat overestimated.

The lower row of Fig. 3 shows the corresponding result for the $d(\nabla \cdot \vec{v})/dt$ -trigger. In this test the $d(\nabla \cdot \vec{v})/dt$ -trigger delivers results that are very similar to the entropy trigger. It provides somewhat less dissipation in the shocked inner region, see Fig. 4, and therefore the velocity distribution there is slightly more noisy.

3.2 Circular Blast

As another benchmark we use a three-dimensional shock-tube problem suggested by Toro (1999). Similar to the Sedov test, we set up 200^3 particles in the computational domain $[-1, 1]^3$. We first place them according to a centroidal Voronoi tessellation (Du et al. 1999) and then perform 500 regularization sweeps. The fluid properties are assigned according to

$$(\rho, \vec{v}, P) = \begin{cases} (1.000, 0, 0, 0, 1.0) & \text{for } r < 0.5 \\ (0.125, 0, 0, 0, 0.1) & \text{else.} \end{cases} \quad (23)$$

The solution exhibits a spherical shock wave, a spherical contact surface traveling in the same direction and a spherical rarefaction wave traveling towards the origin. Our solution (xy -plane) at $t = 0.2$ is shown in Fig. 5 with dissipation parameter α (left), density ρ , velocity v and pressure P . While the "glass-like" initial particle distribution leaves some weak imprint on the α -values (left panel) all the physical quantities (panels 2-4) are essentially perfectly spherically symmetric. The comparison of the MAGMA2-result ($|y| < 0.018, |z| < 0.018$) with the reference solution obtained with the Eulerian weighted average flux method with 400^3 grid cells (Toro 1999) shows a very good agreement between both, see Fig. 6, upper row. In the lower row of this figure we show the $d(\nabla \cdot \vec{v})/dt$ -trigger results. Again the agreement is very good, but since less dissipation is triggered there are larger velocity overshoots at the shock front.

3.3 Schulz-Rinne tests

Schulz-Rinne (1993) designed a set of challenging 2D Riemann problems in which four constant states meet at one corner. The initial conditions are chosen so that one elementary wave, either a shock, a rarefaction or a contact discontinuity emerges from each interface and the subsequent evolution leads to geometrically complex solutions. No exact solutions are known, but the benchmark tests are often used and the results can be compared to other numerical solutions (Schulz-Rinne 1993; Lax & Liu 1998; Kurganov & Tadmor 2002; Liska & Wendroff 2003). Here we show the results for two such tests, the initial conditions of which are given in Tab. 1. Further tests of this type are shown in the MAGMA2 code paper (Rosswog 2020)³.

These tests are rarely shown for SPH codes, in fact, we are only

² Note that their kernels have a support radius of $1h$ while we follow the convention that the kernel is non-zero out to a radius of $2h$.

³ The tests shown here are test 3 and 12 in the numbering of Kurganov & Tadmor (2002).

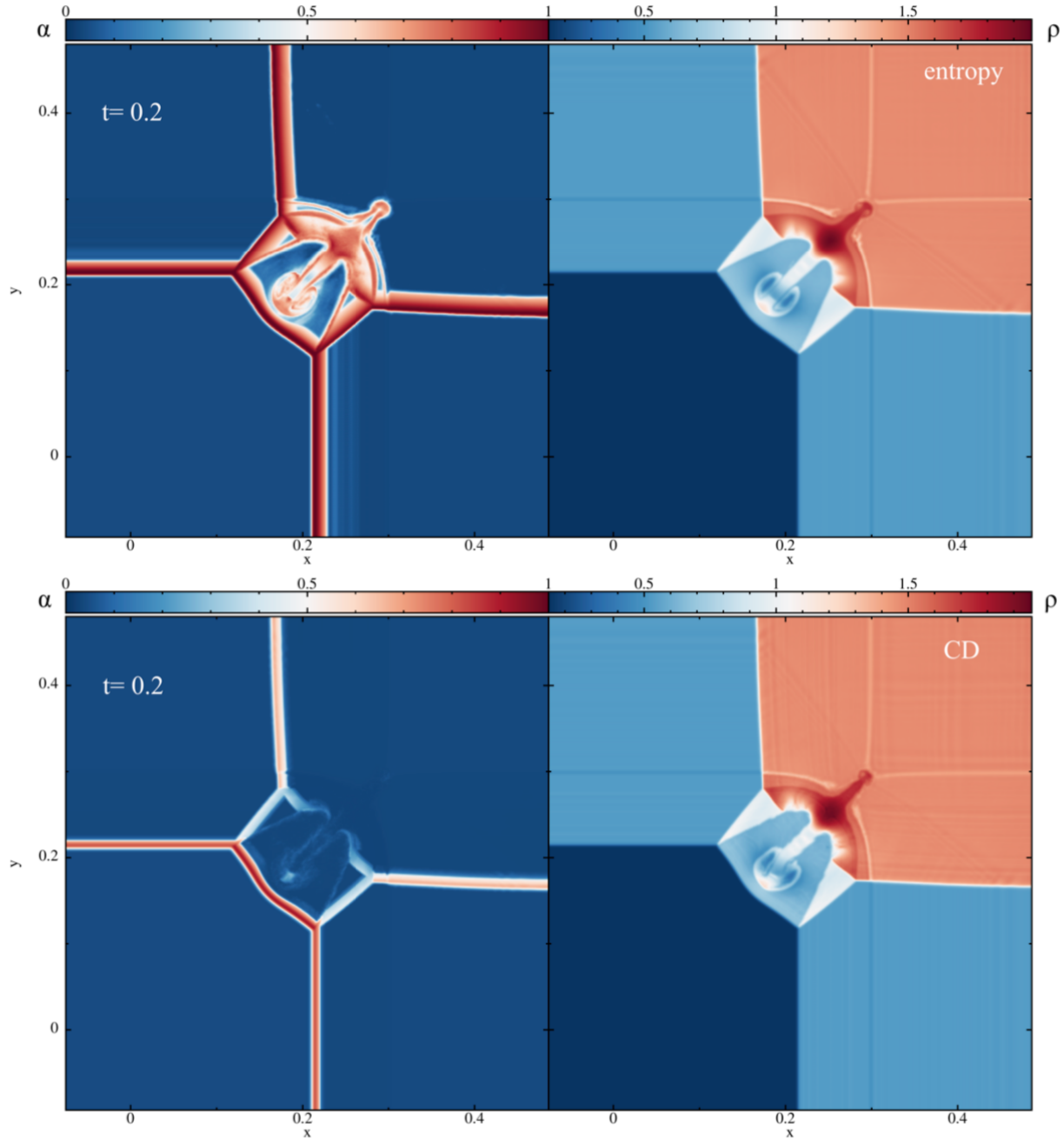


Figure 7. Schulz-Rinne test 1 with the suggested entropy steering (top row) and the $d(\nabla \cdot \vec{v})/dt$ -trigger (bottom row, "CD"). In each row the dissipation parameter α is shown on the left and the density ρ on the right. Note the emerging asymmetries in the density in the bottom row since too little dissipation is triggered.

aware of the work by Puri & Ramachandran (2014) who show results for one such shock test in a study of Godunov-SPH with different approximate Riemann solvers. Most of their implementations, however, show serious artefacts in this test. Since our code is intrinsically 3D, we simulate a slice thick enough so that the midplane is unaffected by edge effects (we use here 10 particle layers in z -direction). We use 660×660 close-packed particles in the xy -plane between $[x_c - 0.5, x_c + 0.5] \times [y_c - 0.5, y_c + 0.5]$, (x_c, y_c) being the contact point of the quadrants, and we use a polytropic exponent $\Gamma = 1.4$.

Fig. 7 shows the results for test SR1 with the upper two panels

showing dissipation parameter α (left) and density (right) for the entropy trigger. The corresponding quantities for the $d(\nabla \cdot \vec{v})/dt$ -trigger are shown in the lower two panels. The general features of the solution are captured in both cases, but the $d(\nabla \cdot \vec{v})/dt$ -trigger provides substantially less dissipation in the central vortex-like region which results in a noticeable lack of symmetry (lower right panel).

The results for the SR2 test are shown in Fig. 8. Again, the results for the entropy trigger are given in the upper panels, those for the $d(\nabla \cdot \vec{v})/dt$ -trigger in the lower ones. The entropy scheme delivers sharp and noise-free density structures with a high degree of sym-

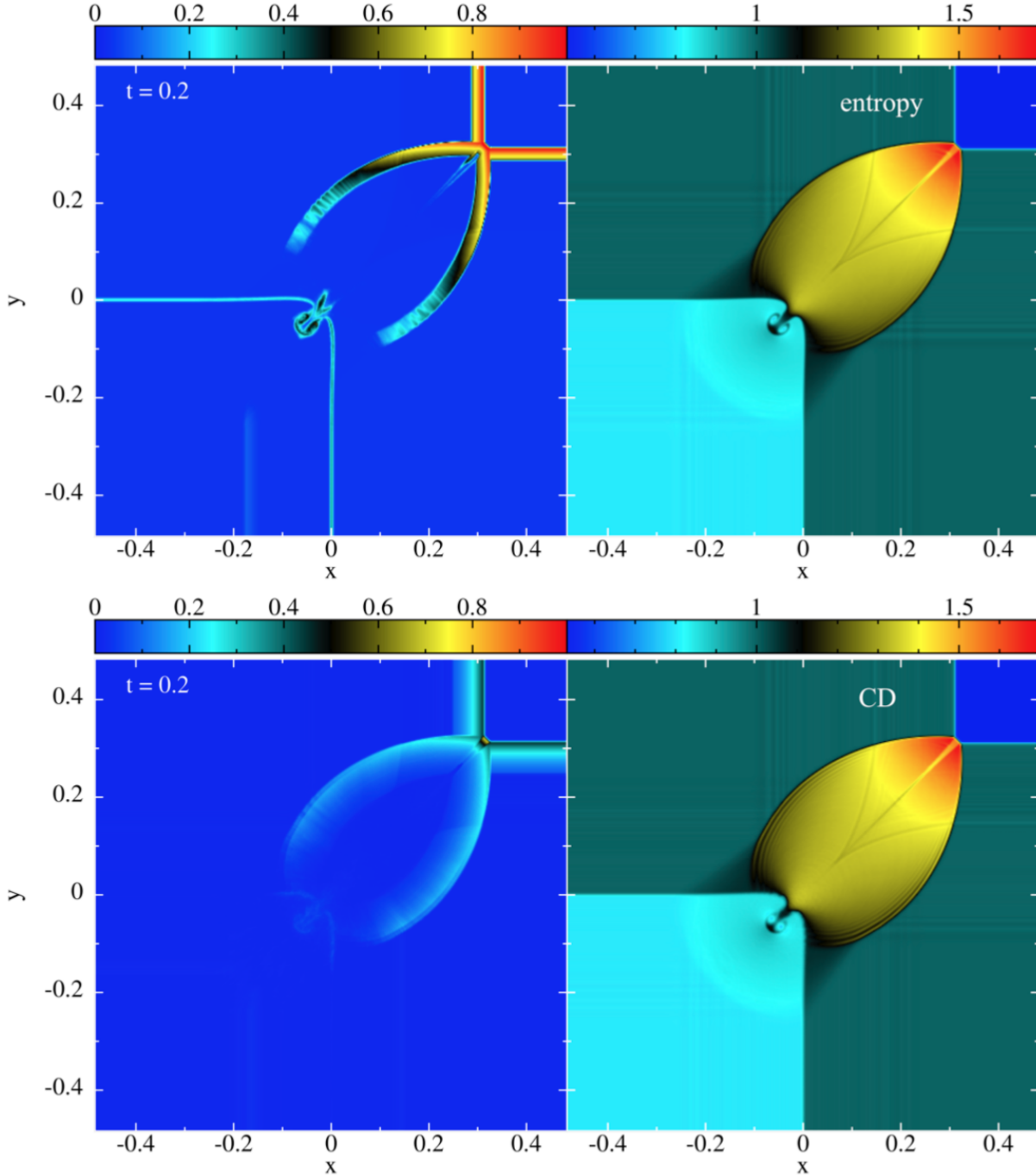


Figure 8. Schulz-Rinne test 2 with the suggested entropy steering (top row) and the scheme suggested by Cullen & Dehnen (2010) (bottom row, "CD"). In each row the dissipation parameter α is shown on the right and density ρ on the left.

metry and that are in very good agreement with the results from Eulerian approaches (Schulz-Rinne 1993; Lax & Liu 1998; Kurganov & Tadmor 2002; Liska & Wendroff 2003). The CD scheme captures the overall features, but again triggers less dissipation which leads to the central vortex structure being substantially less developed.

3.4 Kelvin Helmholtz

An interesting question is how much dissipation is triggered in an overall smooth test such as a Kelvin-Helmholtz instability. To find out we set up a test similar to McNally et al. (2012) and Frontiere et al. (2017). The test is initialized as:

$$\rho(y) = \begin{cases} \rho_1 - \rho_m e^{(y-0.25)/\Delta} & \text{for } 0.00 < y < 0.25 \\ \rho_2 + \rho_m e^{(0.25-y)/\Delta} & \text{for } 0.25 \leq y < 0.50 \\ \rho_2 + \rho_m e^{(y-0.75)/\Delta} & \text{for } 0.50 \leq y < 0.75 \\ \rho_1 - \rho_m e^{(0.75-y)/\Delta} & \text{for } 0.75 \leq y < 1.00 \end{cases} \quad (24)$$

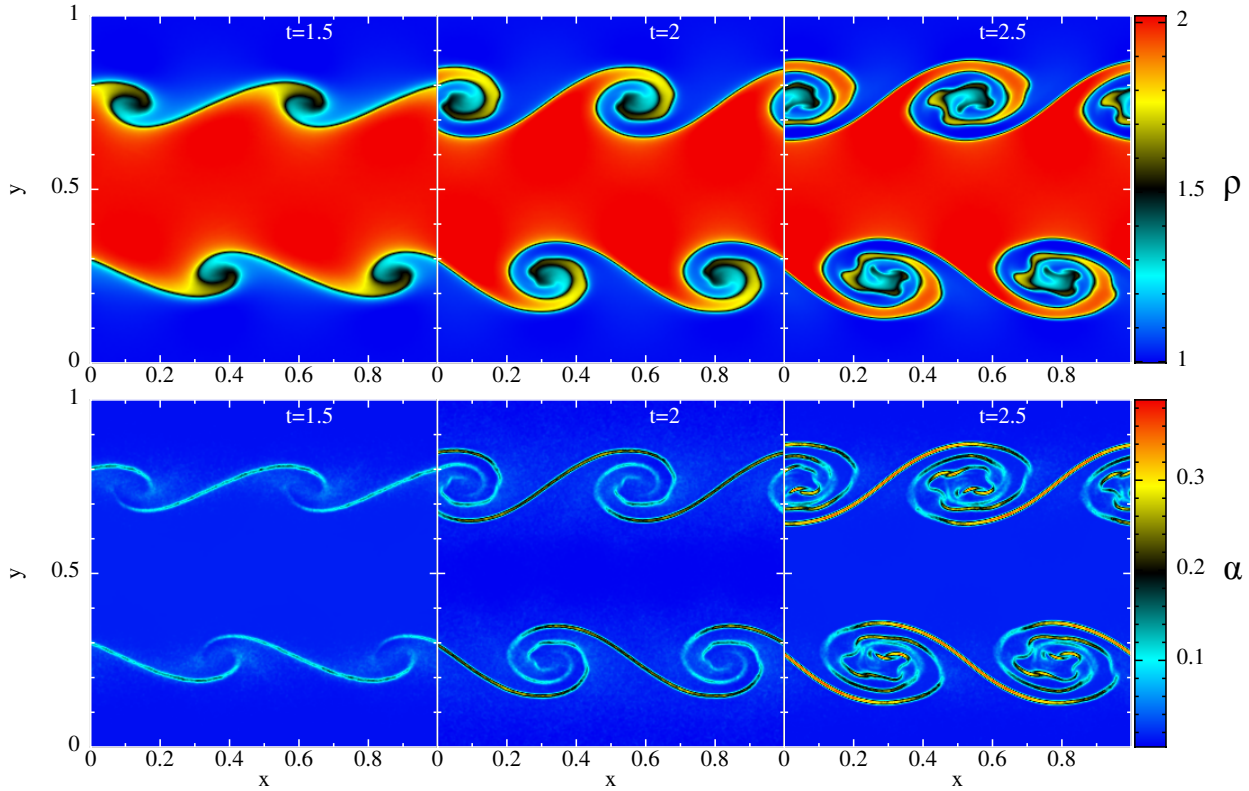


Figure 9. Kelvin-Helmholtz test, density ρ is shown in top, dissipation parameter α in the bottom row.

Table 1. Initial data for the Schulz-Rinne-type 2D Riemann problems

SR1; contact point: (0.3, 0.3)				
variable	NW	NE	SW	SE
ρ	0.5323	1.5000	0.1380	0.5323
v_x	1.2060	0.0000	1.2060	0.0000
v_y	0.0000	0.0000	1.2060	1.2060
P	0.3000	1.5000	0.0290	0.3000
SR2; contact point: (0.0, 0.0)				
variable	NW	NE	SW	SE
ρ	1.0000	0.5313	0.8000	1.000
v_x	0.7276	0.0000	0.0000	0.0000
v_y	0.0000	0.0000	0.0000	0.7262
P	1.0000	0.4000	1.0000	1.0000

where $\rho_1 = 1$, $\rho_2 = 2$, $\rho_m = (\rho_1 - \rho_2)/2$ and $\Delta = 0.025$ and the initial velocities are

$$v_x(y) = \begin{cases} v_1 - v_m e^{(y-0.25)/\Delta} & \text{for } 0.00 < y < 0.25 \\ v_2 + v_m e^{(0.25-y)/\Delta} & \text{for } 0.25 \leq y < 0.50 \\ v_2 + v_m e^{(y-0.75)/\Delta} & \text{for } 0.50 \leq y < 0.75 \\ v_1 - v_m e^{(0.75-y)/\Delta} & \text{for } 0.75 \leq y < 1.00 \end{cases} \quad (25)$$

with $v_1 = 0.5$, $v_2 = -0.5$, $v_m = (v_1 - v_2)/2$. A small velocity perturbation in y -direction is introduced as $v_y = 0.01 \sin(2\pi x/\lambda)$ with the perturbation wave length $\lambda = 0.5$. The test is performed with a polytropic equation of state with exponent $\Gamma = 5/3$. The test is set up in quasi-2D with 20 slices of 512×512 particles which, for simplic-

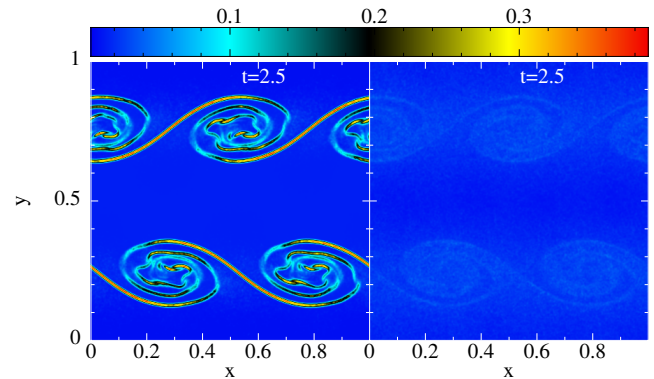


Figure 10. Comparison of the dissipation values α triggered by the entropy (left) and the $d(\nabla \cdot \bar{v})/dt$ -method (right).

ity, are arranged in a simple cubic lattice. Here we focus exclusively on the topic of this paper, the dissipation trigger, for more details of the setup and the analysis of the MAGMA2 performance we refer to Rosswog (2020). The result at $t = 1.5, 2.0$ and 2.5 is shown in Fig. 9. Our dissipation scheme triggers a floor value of $\alpha \approx 0.015$. In the shear interfaces where the particle lattices shear along one another sharply localized lines with values of up to $\alpha \approx 0.4$ are triggered. The average dissipation parameter value at $t = 2.5$ is $\bar{\alpha} = 0.09$, i.e. the α -values are substantially lower than the standard value of unity.

We have repeated this test with the $d(\nabla \cdot \bar{v})/dt$ -trigger. The density evolution is visually very similar to the one shown in Fig. 9, the

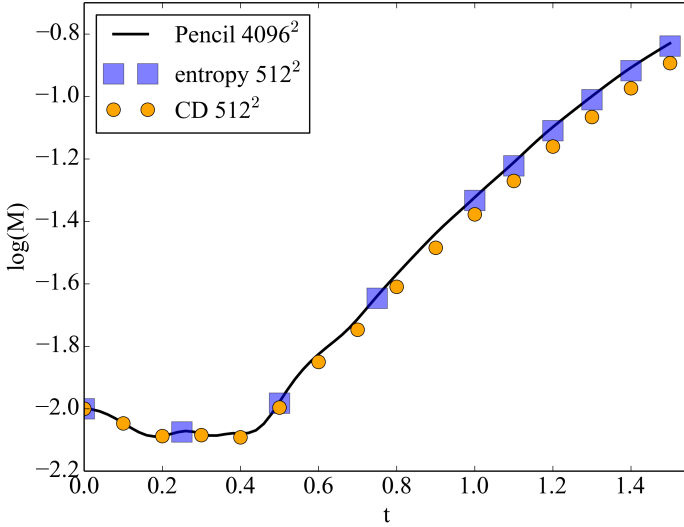


Figure 11. Kelvin-Helmholtz rate calculated as in McNally et al. (2012). The growth rate with the suggested entropy trigger is shown as blue squares (“entropy”), with the $d(\nabla \cdot \vec{v})/dt$ -trigger as orange (“CD”). As reference solution we take a high resolution (4096^2 grid cells) simulation from the Pencil code.

only noticeable difference is that the Kelvin-Helmholtz billows at late times are less symmetric than for the entropy trigger. The α values (at $t = 2.5$) are shown in Fig. 10: the $d(\nabla \cdot \vec{v})/dt$ method hardly switches on anywhere and reaches even in the Kelvin-Helmholtz billows only values of $\alpha \sim 0.03$. We have also measured the growth rate of the instability, calculated exactly as in McNally et al. (2012). As a reference solution we use a high resolution calculation (4096^2 cells) obtained by the PENCIL code (Brandenburg & Dobler 2002). Both our cases show a healthy growth rate, but the entropy method is noticeably closer to the reference solution, likely because noise is more efficiently suppressed.

3.5 Rayleigh-Taylor Instability

As a last example we show the results for a commonly used Rayleigh-Taylor test (Abel 2011; Hopkins 2015; Frontiere et al. 2017). Again, the focus is on the amount of dissipation that is triggered, more details on this test can be found in original code paper (Rosswog 2020). We adopt a quasi-2D setup using the full 3D code in a xy -domain of $[-0.25, 0.25] \times [0, 1]$ and use 10 layers of particles in the z -direction. The initial density is set up as

$$\rho(y) = \rho_b + \frac{\rho_t - \rho_b}{1 + \exp[-(y - y_t)/\Delta]} \quad (26)$$

with $\rho_t = 2$, $\rho_b = 1$, transition width $\Delta = 0.025$ and transition coordinate $y_t = 0.5$. The interface is perturbed as

$$v_y(x, y) = \delta v_{y,0} [1 + \cos(8\pi x)] [1 + \cos(5\pi(y - y_t))] \quad (27)$$

for y in $[0.3, 0.7]$ with an initial amplitude $\delta v_{y,0} = 0.025$. The equilibrium pressure profile is given by

$$P(y) = P_0 - g\rho(y)[y - y_t], \quad (28)$$

where $P_0 = \rho_t/\Gamma$ and polytropic exponent is chosen as $\Gamma = 1.4$. A constant acceleration $\vec{g} = -0.5\hat{e}_y$ is applied. We show snapshots at $t = 2.8, 3.4$ and 4.0 in Fig. 12 with density in the upper row and the

corresponding dissipation parameters in the lower row. Throughout most of the computational domain the value of α is very low (~ 0.01), only in the sharp edges of the rising plumes values up to ≈ 0.7 are reached. Overall, our results in this test are very similar to those obtained with Lagrangian finite volume particle methods (Hopkins 2015) and SPH-methods (Frontiere et al. 2017) based on the reproducing kernel methodology (Liu et al. 1995).

We have repeated this test with the $d(\nabla \cdot \vec{v})/dt$ -trigger. We find that it actually triggers more dissipation in this test than the new approach, see Fig. 13, right panels, but the effects are benign since the evolution (at least with our approach) is not very sensitive to the exact values of α . Visually, the density evolution (left panels) is very similar between the two approaches. We further compare, more quantitatively, the position of the fluid interface in the central rising and the down-sinking parts of the flow. Practically, we use bisections to track the density value $(\rho_t + \rho_b)/2 = 1.5$ along the y -axis, y_{rise} , and along $x = 0.125$ (the right down-sinking “mushroom”), y_{fall} , to capture the interface positions. These interface positions are shown in Fig. 14, but, as expected from Fig. 13, there are hardly any differences noticeable.

4 SUMMARY

In this paper we have explored a novel way to steer dissipation in SPH simulations. Rather than triggering on the velocity divergence (Morris & Monaghan 1997) or its time derivative (Cullen & Dehnen 2010), we trigger on local violations of exact entropy conservation. Such violations can be caused by particles entering a shock front or by numerical noise. We find the additional triggering on noise very beneficial in calming down post-shock regions and in resolving complex fluid structures as they emerge e.g. in Schulz-Rinne test cases. Triggers on noise, in addition to a shock trigger, had been suggested in earlier work (Rosswog 2015a), but the new scheme discussed here is much simpler and the same triggering mechanism takes care of both shocks and noise. The new scheme switches on robustly in shocks, moderately and only very locally in the case of noise and it triggers hardly any dissipation ($\alpha \sim 0.01$ for our parameter choice) in smooth regions of the flow. The suggested method is very robust, trivial to implement in existing SPH codes and does not require any noticeable computational effort.

ACKNOWLEDGEMENTS

Some of the figures of this article were produced with the visualization software SPLASH (Price & Monaghan 2007). This work has been supported by the Swedish Research Council (VR) under grant number 2016-03657_3, by the Swedish National Space Board under grant number Dnr. 107/16 and by the research environment grant “Gravitational Radiation and Electromagnetic Astrophysical Transients (GREAT)” funded by the Swedish Research Council (VR) under Dnr 2016-06012. We gratefully acknowledge support from COST Action CA16104 “Gravitational waves, black holes and fundamental physics” (GWverse) and from COST Action CA16214 “The multi-messenger physics and astrophysics of neutron stars” (PHAROS). The simulations for this paper were performed on the facilities of the North-German Supercomputing Alliance (HLRN), and on the SNIC resources Tetralith and Beskow.

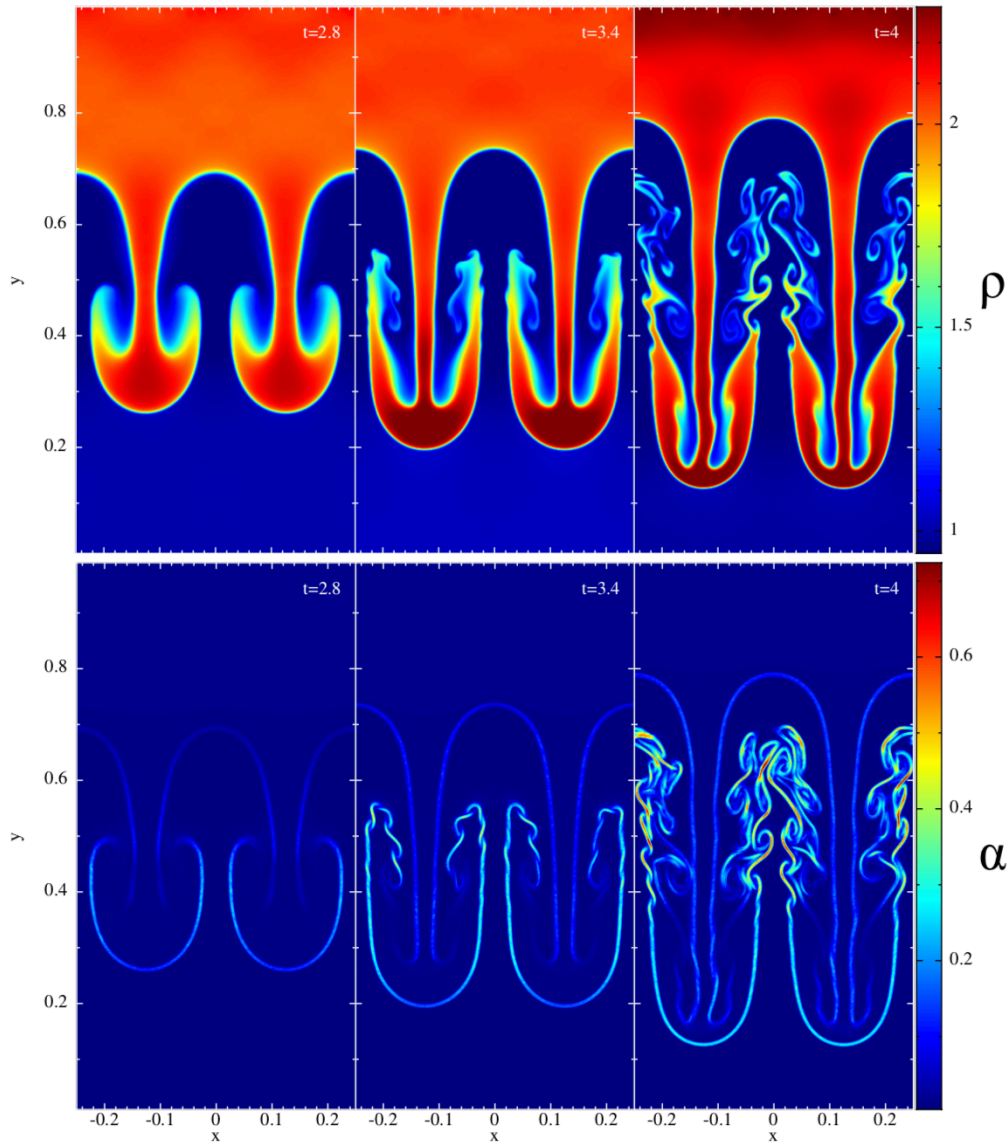


Figure 12. Rayleigh-Taylor test (512×1024 particles). The top row shows the density ρ and bottom row the evolution of the dissipation parameter α triggered by the suggested entropy criterion.

REFERENCES

- Abel T., 2011, *MNRAS*, 413, 271
 Balsara D., 1995, *J. Comput. Phys.*, 121, 357
 Brandenburg A., Dobler W., 2002, *Computer Physics Communications*, 147, 471
 Cabezon R. M., Garcia-Senz D., Escartin J. A., 2012, *A & A*, 545, A112
 Cardall C. Y., Budiardja R. D., Endeve E., Mezzacappa A., 2014, *ApJS*, 210, 17
 Cha S.-H., Whitworth A. P., 2003, *MNRAS*, 340, 73
 Christensen R. B., 1990, *Nuclear Explosives Code Developers Conference*, volume UCRL-JC-105269. Lawrence Livermore National Lab, Lawrence Livermore Technical Report., UCRL-JC-105269
 Cullen L., Dehnen W., 2010, *MNRAS*, 408, 669
 Du Q., Faber V., Gunzburger M., 1999, *SIAM Review*, 41, 637
 Frontiere N., Raskin C. D., Owen J. M., 2017, *Journal of Computational Physics*, 332, 160
 Gaburov E., Nitadori K., 2011, *MNRAS*, 414, 129
 Garcia-Senz D., Cabezon R., Escartin J., 2012, *A & A*, 538, A9
 Gingold R. A., Monaghan J. J., 1982, *Journal of Computational Physics*, 46, 429
 Guercilena F., Radice D., Rezzolla L., 2017, *Computational Astrophysics and Cosmology*, 4, 3
 Guermond J.-L., Pasquetti R., Popov B., 2011, *Journal of Computational Physics*, 230, 4248
 Guermond J.-L., Popov B., Tomov V., 2016, *Computer Methods in Applied Mechanics and Engineering*, 300, 402
 Hopkins P. F., 2015, *MNRAS*, 450, 53
 Hu C.-Y., Naab T., Walch S., Moster B. P., Oser L., 2014, *ArXiv e-prints*
 Inutsuka S.-I., 2002, *Journal of Computational Physics*, 179, 238
 Kurganov A., Tadmor E., 2002
 Lax P., Liu X., 1998, *SIAM J. Sci. Comput.*, 19, 319
 Liska R., Wendroff B., 2003, *SIAM J. Sci. Comput.*, 25, 995

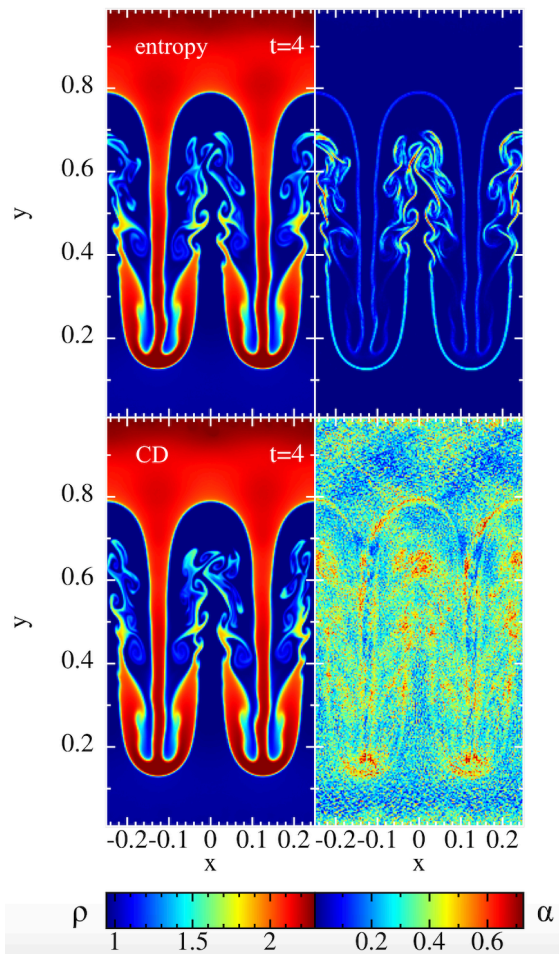


Figure 13. Comparison of the triggered dissipation parameter values, entropy trigger (top) and $d(\nabla \cdot \bar{v})/dt$ -trigger (bottom).

- Liu W. K., Jun S., Zhang Y. F., 1995, *International Journal for Numerical Methods in Fluids*, 20, 1081
 Lucy L., 1977, *The Astronomical Journal*, 82, 1013
 McNally C. P., Lyra W., Passy J.-C., 2012, *ApJS*, 201, 18
 Monaghan J., 1977, *M.N.R.A.S.*, 181, 375
 Monaghan J., Gingold R., 1983, *J. Comp. Phys.*, 52, 374
 Monaghan J. J., 1997, *Journal of Computational Physics*, 136, 298
 Monaghan J. J., Price D. J., 2001, *MNRAS*, 328, 381
 Morris J., Monaghan J., 1997, *J. Comp. Phys.*, 136, 41
 Owen J. M., 2004, *Journal of Computational Physics*, 201, 601
 Price D., Monaghan J., 2007, *MNRAS*, 374, 1347
 Puri K., Ramachandran P., 2014, *Journal of Computational Physics*, 270, 432
 Read J. I., Hayfield T., 2012, *MNRAS*, 422, 3037
 Rosswog S., 2015a, *MNRAS*, 448, 3628
 Rosswog S., 2015b, *Living Reviews of Computational Astrophysics* (2015), 1
 Rosswog S., 2020, arXiv e-prints, p. arXiv:1911.13093
 Rosswog S., Davies M. B., Thielemann F.-K., Piran T., 2000, *A&A*, 360, 171

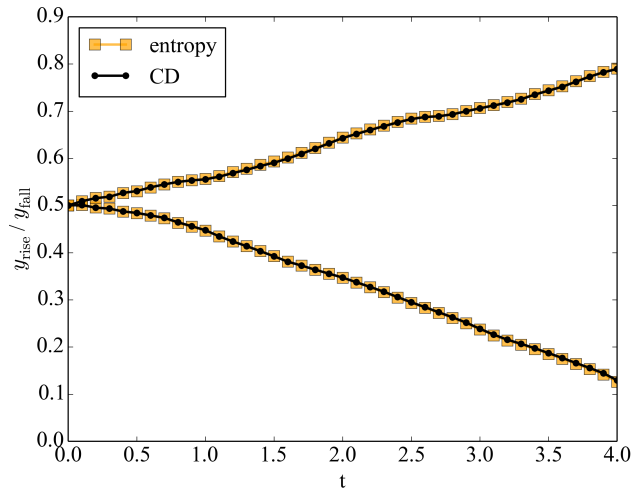


Figure 14. Measure of the y - positions of the density interface in the rising (at $x = 0$, y_{rise}) and down-sinking part of the flow (at $x = 0.125$, y_{fall}) for both the entropy- (orange) and the $d(\nabla \cdot \bar{v})/dt$ -steering (black).

- Rosswog S., Price D., 2007, *MNRAS*, 379, 915
 Schulz-Rinne C. W., 1993, *SIAM Journal of Mathematical Analysis*, 24, 76
 Speith R., 1998, PhD thesis, Eberhard-Karls-Universität Tübingen
 Springel V., Hernquist L., 2002, *MNRAS*, 333, 649
 Toro E., 1999, *Riemann Solvers and Numerical Methods for Fluid Dynamics*. Springer, Berlin
 Tricco T. S., 2019, *MNRAS*, 488, 5210
 van Leer B., 1974, *Journal of Computational Physics*, 14, 361
 von Neumann J., Richtmyer R. D., 1950, *Journal of Applied Physics*, 21, 232
 Wadsley J. W., Keller B. W., Quinn T. R., 2017, *MNRAS*, 471, 2357
 Wendland H., 1995, *Advances in Computational Mathematics*, 4, 389